Catena 93 (2012) 18–28

Contents lists available at SciVerse ScienceDirect

Catena

journal homepage: www.elsevier.com/locate/catena

Spatial variations of soil weathering processes in a tropical mountain environment: The Baturité massif and its piedmont (Ceará, NE Brazil)

François Bétard

Université Paris-Diderot, Sorbonne Paris Cité, Laboratoire PRODIG, UMR 8586 CNRS, F-75205 Paris, France

ARTICLE INFO

Article history:
Received 3 April 2011
Received in revised form 5 January 2012
Accepted 26 January 2012
Available online xxxx

Keywords:
Weathering
Saprolite
Grus
Water balance
Tropical climate
Brazil

ABSTRACT

Strong spatial variations in soil weathering processes were identified in the uplands and piedmont zones of the Baturité massif (Ceará, NE Brazil), a medium-elevation tropical mountain characterized by a steep ecocline between humid climate of the summit zone and semi-arid conditions of the erosional piedmont. With the combined help of field surveys and laboratory analyses, involving micromorphological observations as well as geochemical and mineralogical investigations, this study demonstrates a close spatial correlation between soil weathering processes and present-day water balance (WBI) variations: (i) in the humid massif ($WBI > 500\ mm \cdot y^{-1}$), monosiallitization is exclusive in soil and upper saprolite horizons and leads to the neoformation of 1:1 clay minerals (well-crystallized kaolinite) with minor amounts of gibbsite; (ii) in the subhumid peripheral area of the massif ($50 < WBI < 500\ mm \cdot y^{-1}$), monosiallitization coexists with bisiallitization in the soil profiles, producing a mixture of 1:1 (kaolinite) and 2:1 (illite) clay minerals along with lower weathering intensity; (iii) in the semiarid piedmont ($0 < WBI < 50\ mm \cdot y^{-1}$), bisiallitization becomes the dominant weathering pathway conducive to grus formation and fersiallitic pedogenesis, with the most vulnerable primary minerals weathered into high-charge, 2:1 clay minerals (smectite and illite). Given that soils and weathering mantles are integrators of "average" bioclimatic conditions that prevail at timescales of 1 to 10 Myr, the distribution of soil weathering signatures in the study area is probably reflective of inevitable, long-term (Quaternary to Neogene) climatic fluctuations around median values close to the present ones. Paleoclimatic legacies inherited from the Paleogene lateritization event are rare, because of the denudation pulse occurring in the Late Tertiary and favoring soil stripping to the paleoweathering front on the erosional piedmont.

1. Introduction

The study of rock weathering and its products concerns various geo-disciplines including soil science, geology, geochemistry, geomorphology and civil engineering, each of which has historically been involved with the description and/or interpretation of weathered materials (Ehlen, 2005). However, most studies focusing on weathering deal with the description and/or dating of vertical variations of weathered materials at the profile scale, i.e. as a function of depth relative to the weathering front (weathered-mantle stratigraphy). Only a few studies bear on spatial variations of soil weathering processes and their controlling factors at the landscape scale (see, e.g., Bourgeon, 2001; Scarciglia et al., 2005; Shaw, 1997); it is yet a key level of organization in understanding many soil-dependant environmental questions addressed at the regional scale, such as biodiversity, water conservation or soil (gully) erosion.

The present investigation focuses on soil and subsurface weathering features of the Baturité massif and its piedmont, one of the humid mountains ("brejos de altitude") rising above the semi-arid plains of the "sertão" in northeastern Brazil (Bétard, 2007). The objectives of the work are (i) to characterize the morphological, geochemical and mineralogical variations in soil properties as a function of topography and climate; (ii) to unravel the forcing factors that control soil weathering processes in this and possibly other tropical mountain environments characterized by steep environmental gradients. Using a wide range of optical, geochemical and mineralogical techniques as well as extensive field surveys, the paper analyses the distribution of soil weathering processes in the regional setting and attempts to relate them to water balance variations in space and time and, possibly, to past climatic and denudational events.

2. Environmental setting

2.1. Topography and geology

Located 80 km southwest of Fortaleza, in the state of Ceará, the study area is part of the northern Brazilian "Nordeste", mostly known for its semiarid environments ("sertão"). Within the wider semiarid matrix of the "sertão", the Baturité massif forms a humid,

E-mail address: francois.betard@univ-paris-diderot.fr.

0341-8162/$ – see front matter © 2012 Elsevier B.V. All rights reserved.
doi:10.1016/j.catena.2012.01.013

isolated mountainous upland with elevations up to 1115 m a.s.l. (Fig. 1). The central part of the massif is characterized by constant elevations around 800–900 m a.s.l., only interrupted by elongated crests and ridges including the highest points above 1000 m a.s.l.. By contrast, elevations in the surrounding plains forming the erosional piedmont do not exceed 200 m a.s.l. The contact between the mountainous massif and the surrounding plains is relatively abrupt, marked by steep slopes and sinuous scarps, especially along the eastern edge where ridges and promontories delineate large reentrants, as around Capistrano, Baturité and Redenção (Fig. 1).

The Baturité massif is interpreted as the erosional remnant of an Early Cretaceous rift shoulder (Peulvast and Claudino Sales, 2004). In the study area, the geological substrate is part of the Central Ceará domain (Monié et al., 1997), between the Senador Pompeu and Sobral Pedro II shear zones. Inside the limits of the study area, the bedrock consists of Proterozoic basement rocks, mainly composed of gneiss with tonalitic to granodioritic compositions (CPRM, 2003). To the east, the piedmont is partly covered by thin, Neogene clastic sediments (Barreiras Formation), interpreted as correlative products of the stripping of Pre-Miocene lateritic paleosaprolites (Bétard, 2007; Gunnell, 1998; Peulvast and Claudino Sales, 2004).

2.2. Present-day climate and vegetation patterns

The present-day climatic conditions are characterized in the whole study area by unimodal rainfall regimes, with a rainy season concentrated on a few months (March to May). Nevertheless, rainfall distribution is orographically induced by the existence of the Baturité massif acting as a mountain barrier exposed to the trade-winds. Temperature gradients are also observed in relation to altitude, with mean annual temperatures ranging between 20 °C in the summit areas of the Baturité massif and 26 °C in the surrounding plains of the "sertão". Three topo-climatic zones can be differentiated (Fig. 1): (i) a humid zone corresponding to the culminating, central part of the massif, with rainfall totals $>1300\ mm \cdot y^{-1}$ and a dry season ≤ 4 months; (ii) a subhumid zone in the peripheral area of the massif, which receives 900 to $1300\ mm \cdot y^{-1}$ for a dry season of 5–6 months; (iii) a semiarid zone, mainly extending on the piedmont, where rainfall is typically $<900\ mm \cdot y^{-1}$ and the dry season >6 months.

In close relation to this topo-climatic framework, the study area exhibits a characteristic vegetation continuum between evergreen forest, or 'mata atlântica', of the humid massif and dry deciduous forest, or 'caatinga', of the semi-arid piedmont, via a semi-deciduous forest belt corresponding to the sub-humid transitional area.

2.3. Geomorphic setting and soil cover

Soil and landform systems of the study area were analysed in detail by Bétard (2007) and provide a basis for analysing the spatial variations of soil weathering processes in the regional setting. Three main soil-landform units related to the above-mentioned bioclimatic zones were recognized and delineated (Fig. 2): (i) the humid massif is characterized by a summit surface (800–900 m a.s.l.) shaped into multiconvex topography supporting Acrisols on the convex hills, and Fluvisols with waterlogging features on the valley bottoms; (ii) the sub-humid peripheral area is typified by highly dissected landscapes (200–800 m a.s.l.), with Lixisols in the hilltops and Leptosols on the eroded slopes of V-shaped valleys; (iii) the semi-arid piedmont (100–200 m a.s.l.) exhibits a typical landscape of pediments and inselbergs covered by Luvisols and Cambisols on wash divides, grading to Planosols and Fluvisols in valley bottoms. To the east, part of the semi-arid piedmont extends the pre-littoral tablelands ("Tabuleiros") which are composed of basal Neogene clastic sediments (Barreiras Formation) covered by paleosols (Lixisols) and of upper Pleistocene aeolian sands underlain by weakly developed soils (Arenosols).

3. Materials and methods

3.1. Field survey and sampling strategy

A detailed pedogeomorphological survey was carried out in the study area, which included a systematic, combined description of mesoscale landforms, weathering features and soil materials (Bétard, 2007). With the help of existing soil profiles and data from the Radambrasil project (Projeto Radambrasil, 1981), many soil profiles were described in the field, along road cuts, quarries and other vertical exposures on the Baturité massif and associated piedmont. Three representative soil profiles (LS1, PA1 and CA1) corresponding to the three main soil-landform units (humid massif, subhumid transitional

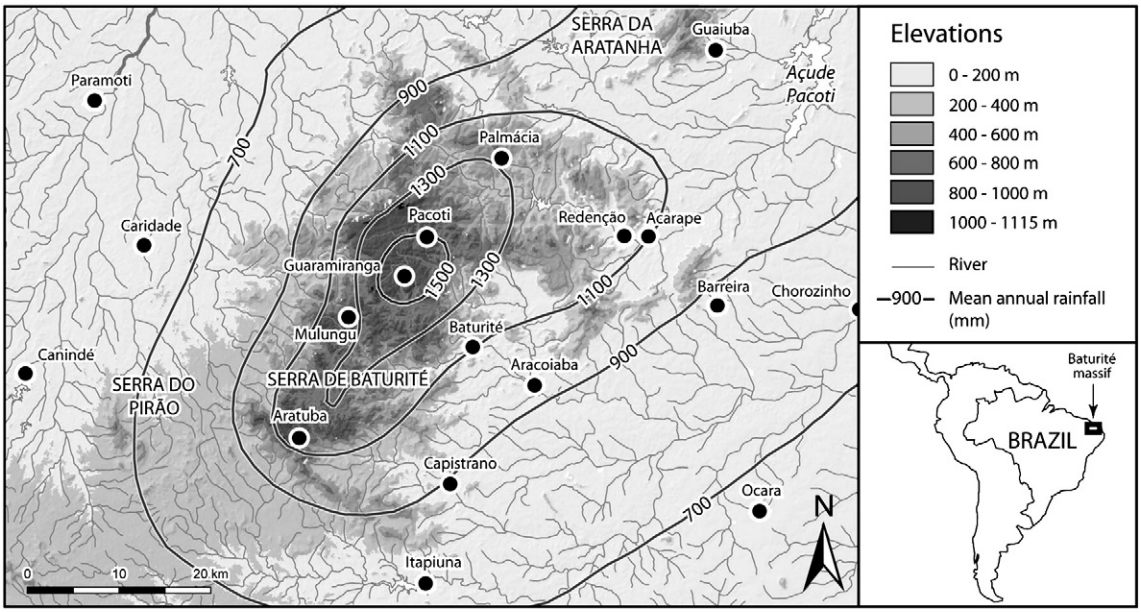

Fig. 1. Environmental setting of the Baturité massif and its piedmont.

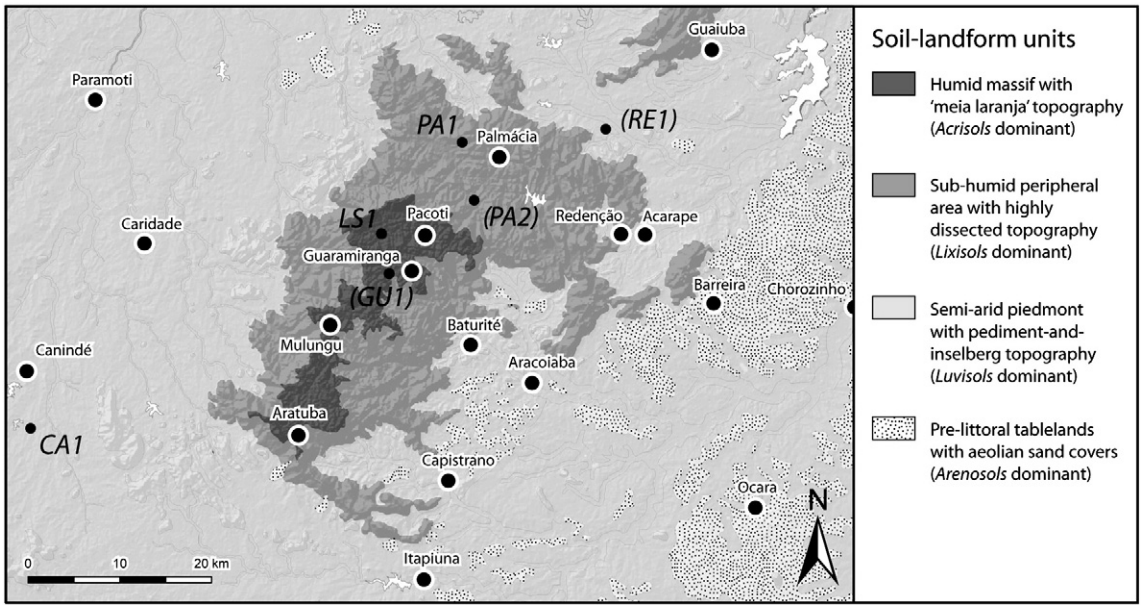

Fig. 2. Simplified soil-landform units of the study area, as mapped by Bétard (2007), and location of selected soil profiles. Secondary profiles are indicated in parenthesis. Soil names follow the World Reference Base for soil resources (IUSS Working Group WRB, 2006).

area and semiarid piedmont: Fig. 2) were selected for detailed sampling at different depths for laboratory analyses. These were completed by the partial sampling of three other (or secondary) profiles (GU1, PA2 and RE1, respectively), in order to verify and/or complete the results obtained from the three main selected profiles. In all cases, the studied sites were suitably selected in similar topographic positions (near-top of interfluves, with slope angles <1°) and on homogenous felsic metamorphic parent rocks (gneiss), which is the dominant lithotype in the Baturité region. Variations at the toposequence scale (from hilltop to valley bottom) were not analysed and illustrated here, as the lower parts of catenas often exhibit colluvium or recent dissection, and are therefore beyond the scope and scale of analysis of this study. Assuming that the study area had been affected by widespread lateritic palaeoweathering in pre-Miocene times (Gunnell, 1998; Tardy and Roquin, 1998), soil profiles displaying such a paleoclimatic imprint (even if rare) were also deliberately avoided in this study, thus focusing on hilltop profiles which are expected to be in dynamic equilibrium with current pedoclimatic conditions.

3.2. Laboratory analyses

Five sets of laboratory analyses were performed in order to characterize the soil weathering processes in the study area: (i) physico-chemical analyses for the global characterization of soils leading to their classification (ii) micromorphological analyses of soil and saprolite samples to analyse their petrology; (iii) total analyses of the bulk material to evaluate the weathering intensity; (iv) selective dissolution procedures to identify the different forms of Fe present in soils and saprolites; and (v) X-ray diffraction (XRD) analyses on powders and <2 μm fraction of soil and weathered materials to characterize their mineralogy.

Samples from each soil and saprolite horizon were air-dried and sieved using a 2 mm round-hole sieve. All physico-chemical analyses were performed on fine earth (<2 mm). Soil pH was measured in suspensions prepared with 10 g of air-dried soil in 25 ml of H_2O and 1 M KCl solutions. Organic carbon was determined by dry combustion using a khatarometer (thermal conductivity). Cation exchange capacity (CEC) and exchangeable bases were determined by the 1 M NH_4OAc method at pH 7.0. Particle-size analysis was performed by the pipette method after pretreatment with H_2O_2 to destroy organic matter and dispersion by Na-hexametaphosphate.

Micromorphological properties were examined using optical microscopy on polished thin sections of 30 μm in thickness, prepared after impregnation with a synthetic resin and hardening of undisturbed samples of weathered rock and saprolite horizons. The objectives of the micromorphological analysis were: (i) to identify primary rock-forming mineral species from weathered and unweathered rock samples, and (ii) to describe their pattern and degree of alteration as well as their weathering products (neoformed clay minerals, amorphous plasma) from corresponding, upper soil and saprolite samples.

Total element analysis of soil and weathered materials were performed on samples of 300 mg of fine earth (<2 mm). Major element concentrations (Si, Al, total Fe, Ti, Mn, Mg, Ca, K, Na and P) were determined using an acid dissolution procedure after lithium metaborate fusion, followed by analysis using inductively coupled plasma-atomic emission spectrometry (ICP-AES). In order to assess and compare the weathering intensity of the different studied profiles, weathering proxies were calculated from major element analyses. Among the weathering indices summarized in Price and Velbel (2003), the Chemical Index of Alteration of Nesbitt and Young (1989) ($CIA = (100)\ [Al_2O_3/(Al_2O_3 + CaO + Na_2O + K_2O)]$) is considered as a reliable proxy of weathering intensity, and one of the most commonly used indexes in studies on weathering mantles. Because Al_2O_3 may be prone to mobility in the tropical weathering environment, a ratio of mobile to immobile elements – the Calcium/Titanium ratio ($CTR = CaO/TiO_2$) – has been used as a complementary weathering index.

Selective dissolution procedures were conducted on samples of fine earth in order to identify the different forms of total Fe (Fe_T), as determined by ICP-AES. Two extractants were used in this study, followed by atomic absorption spectrophotometry for determination of the respective iron contents: (i) dithionite-bicarbonate-citrate (DBC) to extract the "free iron" (crystalline Fe oxides and amorphous constituents: Fe_d) (Mehra and Jackson, 1960); (ii) ammonium oxalate buffered to pH 3 with oxalic acid, to isolate the poorly crystallized forms of Fe (amorphous and para-crystalline constituents: Fe_o) (Blakemore et al., 1987). Thus the difference ($Fe_d - Fe_o$) can then be used to estimate the content of well crystallized Fe oxides in the fine earth of the weathering mantles. Combined with the interpretation of CIA and CTR values, the calculation of different ratios – e.g.

Fe_d/Fe_T which determines the percentage of free iron – may help in the global appreciation of weathering intensity.

Mineralogy of the soil profiles was assessed from powder X-ray diffraction of bulk saprolite and soil samples using a PANALYTICAL XPert diffractometer, with a large scanning ranging from 2.5 and 65° 2θ. In order to assess the clay mineralogy of alteration products, X-ray diffractograms of the <2 μm fraction were obtained using a SIEMENS Kristalloflex D500 diffractometer. These samples were analysed on oriented glass slides in both air-dried (AD) and glycolated (EG) states, and were scanned from 2.5 to 25° 2θ with a time step of 0.02° 2θ and a counting time of 5 s. Other chemical and thermal treatments were performed on some samples for detailed XRD analysis, e.g. K-saturation at room temperature with a 1 M KCl, followed by heating at 110, 330 and 550 °C.

3.3. Water balance index (WBI)

Assuming that only a part of the total rainfall is effective for weathering, it was necessary to proceed with water balance calculations to quantify the deep percolation into the weathering system, in order to further appreciate its possible influence on the spatial variations observed in soil-weathering facies as a function of climate. To achieve this, we used a water balance index (namely the "climatic drainage") proposed by Bourgeon and Pédro (1992) who have shown its effectiveness to analyse the climatic control on weathering processes in tropical regions. According to these authors, the "climatic drainage" is an estimation of the amount of water which percolates through the soil profile beyond 1 m depth. The calculation of the water balance index (WBI) was based on a 1974–2004 time series of monthly climatic data according to the following formula:

$$\mathrm{WBI} = \sum\left[(\mathrm{P–PET})_{\mathrm{month}}\right] – 100, \text{ for } (\mathrm{P–PET})_{\mathrm{month}} > 0,$$

where P is precipitation and PET is potential evapotranspiration calculated following the Thornthwaite formula. A deduction of 100 mm is conventionally applied to take into account the yearly water storage capacity of the upper soil horizons. The "climatic drainage" was computed for 18 stations of the study area, year by year, allowing frequency-domain calculations by establishing annual median values along with the magnitude of deviations from these values (1st and 3rd quartiles). Such a statistical approach allowed a better appreciation of the water-balance interannual variability. Spatialisation of the WBI was made possible by the integration and interpolation of the climatic data set into a Geographic Information System (GIS) using ArcGIS 9.1 (Fig. 3). WBI envelopes represented on the map were accordingly defined to encompass the three main soil-landform units and related climatic zones: (i) the humid massif ($P > 1300\ mm \cdot y^{-1}$; $WBI > 500\ mm \cdot y^{-1}$); (ii) the subhumid transition area ($900 < P < 1300\ mm \cdot y^{-1}$; $50 < WBI < 500\ mm \cdot y^{-1}$) and (iii) the semiarid piedmont ($P < 900\ mm \cdot y^{-1}$; $0 < WBI < 50\ mm \cdot y^{-1}$).

4. Results

4.1. Soil and subsurface weathering facies of the humid massif ($WBI > 500\ mm \cdot y^{-1}$)

4.1.1. Profile morphology and chemistry

The LS1 soil profile is located at 6 km to the northwest of Guaramiranga, in the core of the multiconvex landscape extending on the humid massif (S 4°14.289′, W 38°58.887′). The profile outcrops along a road cut at the top of a convex hill (or "half orange") occupied by evergreen forest, at 900 m a.s.l. (Fig. 4a). Below the organic horizon A1 and the stone-line occurring at ~1 m depth, a Bt (argic) horizon, with clay coatings and high clay contents, suggests an active argilization process. A discontinuous BC horizon forms the transition with the red-coloured fine saprolite (C horizon) of sandy-clay texture and massive structure.

Soil pH indicates high levels of acidity, with H_2O pH values <5 in all soil horizons (Table 1). A low cation-exchange capacity (<24 cmol (+) kg^{-1} of clay), combined with a low base saturation, indicates high degree of lixiviation and weathering in the soil horizons. Profile LS1 classifies as a Cutanic Acrisol (humic) (IUSS Working Group WRB, 2006).

4.1.2. Micromorphological characterization of weathering

Micromorphological observations of the fine saprolite (C horizon) show that the main primary rock-forming minerals of the gneiss (K-feldspars, plagioclases and biotites) are intensely weathered, with the exception of quartz and muscovite (Fig. 4b). The less resistant mineral species are entirely replaced by brown amorphous plasma responsible for the very friable dry consistence of the saprolite.

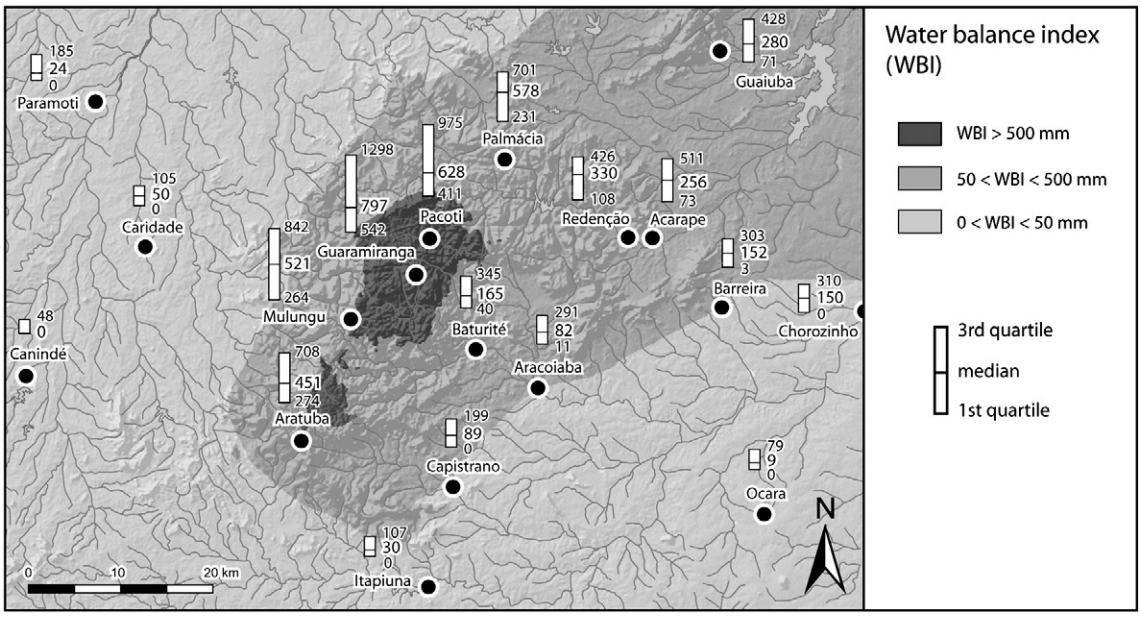

Fig. 3. Water balance index (WBI) map.

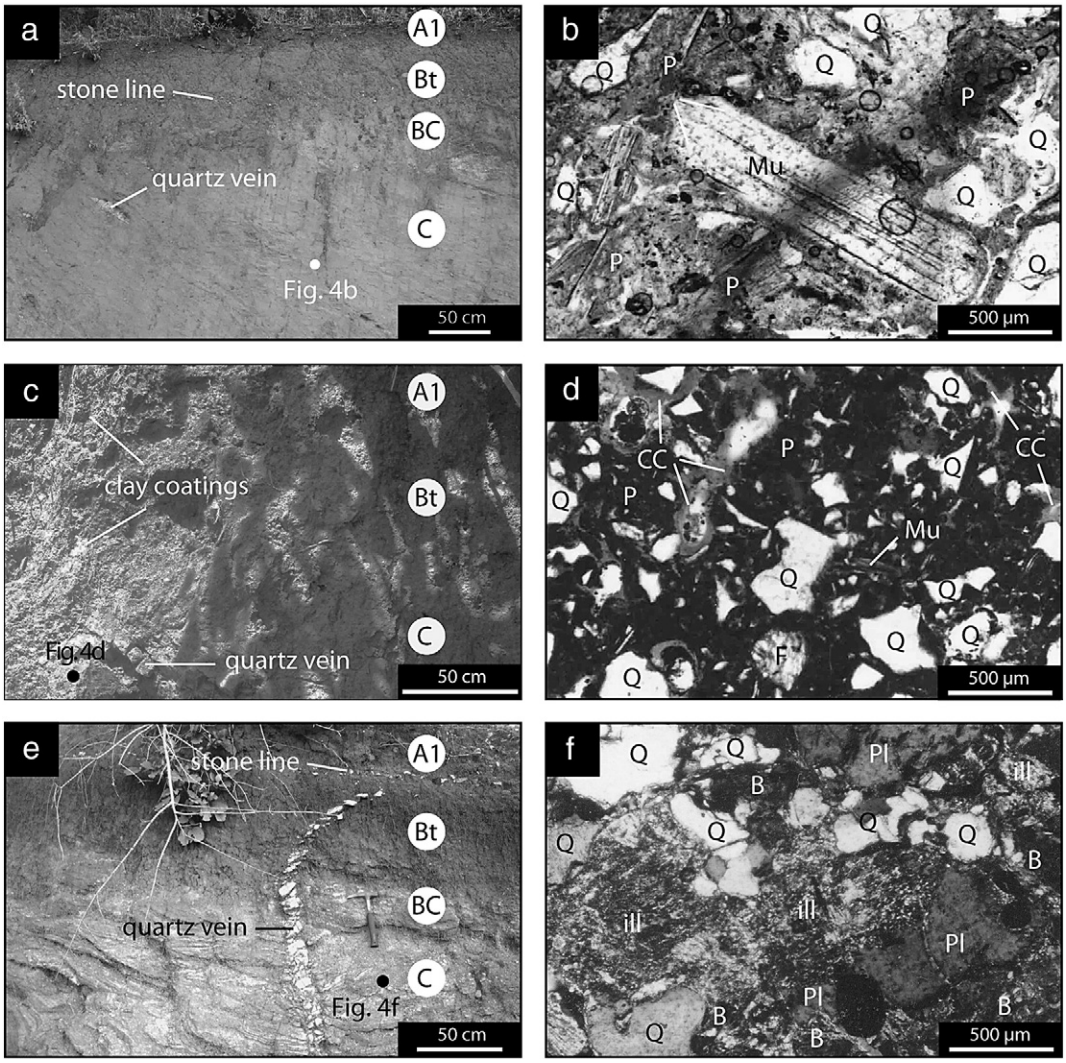

Fig. 4. Macro- and micromorphological features of selected soil profiles in the Baturité massif and associated piedmont: (a) macromorphological features of profile LS1 (humid massif); (b) micromorphological features of profile LS1 at 260 cm depth; (c) macromorphological features of profile PA1 (subhumid transitional area); (d) micromorphological features of profile PA1 at 150 cm depth; (e) macromorphological features of profile CA1 (semi-arid piedmont); (f) micromorphological features of profile CA1 at 135 cm depth. Symbols on (b), (d) and (f): Q: quartz; Mu: muscovite; F: K-feldspar; Pl: plagioclase; B: biotite; CC: clay coating; P: amorphous plasma; ill: illite.

Table 1
Morphological and chemical characteristics of the investigated soil profiles.

Depth (cm)	Horizon	Color (moist)	Textural classes[a]	Structure	Clay ($g.kg^{-1}$)	Org. C ($g.kg^{-1}$)	pH H_2O	pH KCl	CEC[b]	Base sat. ratio
Profile LS1 – S 4°14.289′, W 38°58.887′ – humid massif										
0–24	A1	7.5YR 4/4	scl	Crumby	326	18.90	4.9	3.9	6.63	15
24–90	B argic	5YR 5/6	c	Subblocky	532	8.20	4.9	4.1	7.37	4
90–160	BC	5YR 6/8	scl	Massive	347	2.77	4.8	4.2	4.26	7
160–360+	C	10R 5/6	ls	Massive	138	3.01	4.8	4.2	2.42	8
Profile PA1 – S 4°08.380′, W 38°50.784′ – subhumid transitional area										
0–30	A1	5YR 4/3	scl	Massive	300	9.71	5.7	4.6	5.98	69
30–60	B argic	2.5YR 3/4	sc	Blocky	436	6.77	5.6	4.3	6.02	79
60–120	B argic	10R 4/8	c	Blocky	479	3.28	5.3	4.2	5.92	55
120–180+	C	10R 4/8	scl	Massive	289	2.23	5.4	4.4	8.21	34
Profile CA1 – S 4°22.301′, W 39°18.271′ – semiarid piedmont										
0–40	A1	7.5YR 4/4	ls	Massive	195	5.52	6.2	4.8	11.16	79
40–75	B argic	5YR 4/4	sc	Blocky	437	6.01	6.2	4.4	19.16	61
75–120	BC	2.5YR 4/6	scl	Massive	282	1.85	6.4	4.3	20.57	66
135	C	variegated	s	Massive	<50	0.86	6.7	4.3	n.d.	n.d.
215	C	variegated	s	Massive	<50	0.33	7.1	4.5	n.d.	n.d.

n.d.: no data.
[a] Textural classes: s, sand; c, clay; ls, loamy sand; sc, sandy clay; scl, sandy clay loam.
[b] Expressed in cmol (+) kg^{-1} of fine earth.

Composed of fine debris of several mineral species mixed with neoformed clay minerals and Fe-oxides, the secondary plasma was observed in the fine saprolite as well as in the upper soil horizons, where the rock structure has been completely disintegrated. In BC and Bt horizons (not illustrated), clay coatings were detected in abundance around weathered crystals of quartz and muscovite, and within the plasmogenic matrix.

4.1.3. Geochemical characteristics and weathering intensity

Geochemical weathering proxies calculated from total element analyses indicate a progressive increase of weathering intensity from deeper saprolite to soil subsurface horizons. Samples collected from profile LS1 show high CIA values, ranging from 89 to 93 (Table 2). The high intensity of chemical weathering led to the removal of the more soluble elements, e.g., MgO, CaO and Na_2O. The relatively high K_2O content is symptomatic of unaltered muscovite crystals still present in the saprolite. CTR values are null in all horizons.

Selective dissolution data and ratios (Table 3) may also be considered as reliable proxies of weathering intensity, in evaluating the relative content of iron released during weathering. The content of DCB extractable Fe, which corresponds to the "free iron", is very high, reaching ~90% of the total Fe in the saprolitic layers. The content and proportion of well crystallized Fe oxides increase with depth, as shown by the difference ($Fe_d - Fe_o$) and the Fe_o/Fe_d ratio, respectively (Table 2), and are maximal in the fine saprolite.

4.1.4. Weathering product mineralogy

Powder XRD data from profile LS1 (not shown) indicate that the most abundant minerals in the fine saprolite are quartz, muscovite, kaolinite and iron oxi-hydroxides (goethite and haematite). X-ray diffractograms of the clay fraction (Fig. 5) confirm the strong prevalence of well crystallized kaolinite (WCK), with a typical elimination of the reflection at 0.715 nm after K-saturation and heating up to 550 °C. The XRD spectra for the same materials also show the presence of well crystallized illite (WCI) with narrow peaks at 1.0 and 0.5 nm, which correspond to the primary micaceous phase (muscovite) inherited from the gneiss parent rock. Gibbsite is only present in trace amounts.

XRD patterns of the <2 μm fraction from a secondary profile (GU1, not illustrated) confirm these mineralogical characteristics by revealing the prevalence of 1:1 minerals (WCK) formed in association with higher contents of gibbsite, whereas WCI was only detected in minute amounts.

Table 3
Selective dissolution data for the characterization of Fe in the investigated soil profiles.

Depth	Fe_T[a]	Fe_d[b]	Fe_o[c]	$Fe_d - Fe_o$	Fe_d/Fe_T	Fe_o/Fe_T	Fe_o/Fe_d
(cm)	(g kg^{-1})	(g kg^{-1})	(g kg^{-1})	(g kg^{-1})	(%)	(%)	(%)
Profile LS1 – S 4°14.289′, W 38°58.887′ – humid massif							
0–24	23.66	18.27	1.65	16.62	77.22	6.47	9.03
24–90	39.76	36.40	1.94	34.46	91.55	4.88	5.33
90–160	25.27	22.37	0.31	22.06	88.52	1.23	1.39
160–360+	55.58	49.66	0.16	49.50	89.35	0.29	0.32
Profile PA1 – S 4°08.380′, W 38°50.784′ – subhumid transitional area							
0–30	21.00	12.70	2.49	10.21	60.48	11.86	19.61
30–60	26.60	19.00	2.15	16.85	71.43	8.08	11.32
60–120	34.86	27.93	2.68	25.25	80.12	7.69	9.60
120–180+	42.21	36.64	2.10	34.54	86.80	4.98	5.73
Profile CA1 – S 4°22.301′, W 39°18.271′ – semiarid piedmont							
0–40	47.88	13.45	0.74	12.71	28.09	1.55	5.50
40–75	57.96	29.19	0.76	28.43	50.36	1.31	2.60
75–120	49.00	20.61	0.43	20.18	42.06	0.88	2.09
135	40.95	8.53	0.27	8.26	20.83	0.66	3.17
215	53.65	7.09	0.30	6.79	13.22	0.56	4.23

[a] Total elemental Fe.
[b] Dithionite-Citrate-Bicarbonate extractable Fe.
[c] Oxalate extractable Fe.

4.2. Soil and subsurface weathering facies of the subhumid transitional area ($50 < WBI < 500\ mm \cdot y^{-1}$)

4.2.1. Profile morphology and chemistry

The PA1 soil profile has been described in a small quarry to the north of Palmacia, in the dissected landscape of the subhumid transitional area (S 4°08.380′, W 38°50.784′). It is located at the upper part of a convexo–concave interfluve at 400 m a.s.l., in a position preserved from active erosion and dissection. The profile comprises an organic horizon A1, an argic horizon (Bt) exhibiting clay coatings, and a fine-textured saprolite (C) with massive structure locally traversed by unaltered quartz veins (Fig. 4c).

In PA1 profile, soil pH is indicative of medium acidity, with H_2O pH values ranging from 5.4 to 5.7 (Table 1). As for profile LS1, the low exchange capacity (<24 cmol (+) kg^{-1} of clay) indicates a predominance of low-activity clays, but the medium to high base saturation (>50) indicates the soil profile PA1 is a Cutanic Lixisol (rhodic) (IUSS Working Group WRB, 2006).

4.2.2. Micromorphological characterization of weathering

As for the soil profiles of the humid massif, the micromorphological features of the fine saprolite (C horizon) are characterized by a total decomposition of the less resistant rock-forming minerals (e.g.,

Table 2
Geochemical characteristics (total analysis of the bulk material) of the investigated soil profiles.

Depth	SiO_2	Al_2O_3	Fe_2O_3	TiO_2	MnO	MgO	CaO	K_2O	Na_2O	P_2O_5	CIA[a]	CTR[b]
(cm)	(g kg^{-1})	(g kg^{-1})	(g kg^{-1})	(g kg^{-1})	(g kg^{-1})	(g kg^{-1})	(g kg^{-1})	(g kg^{-1})	(g kg^{-1})	(g kg^{-1})		
Profile LS1 – S 4°14.289′, W 38°58.887′ – humid massif												
0–24	755.4	113.3	33.8	5.6	0.1	1.1	0.0	9.8	0.0	0.5	92.07	0.00
24–90	647.8	171.0	56.8	7.4	0.1	1.3	0.0	11.6	0.0	0.5	93.64	0.00
90–160	623.2	226.4	36.1	3.5	0.1	1.3	0.0	17.9	0.7	3.5	92.40	0.00
160–360+	637.4	180.5	79.4	12.2	0.2	1.9	0.0	20.4	0.9	1.3	89.44	0.00
Profile PA1 – S 4°08.380′, W 38°50.784′ – subhumid transitional area												
0–30	736.8	129.3	30.0	4.8	0.5	1.7	1.3	24.7	2.4	0.6	81.96	27.08
30–60	688.6	161.8	38.0	5.1	0.3	1.9	1.0	21.7	1.7	0.5	86.90	19.61
60–120	656.7	183.3	49.8	5.9	0.2	2.2	0.5	16.1	0.8	0.6	91.39	8.47
120–180+	702.3	143.6	60.3	7.6	0.1	3.3	0.4	11.5	0.0	0.7	92.38	5.13
Profile CA1 – S 4°22.301′, W 39°18.271′ – semiarid piedmont												
0–40	654.6	148.5	68.4	7.6	0.9	13.6	16.9	18.2	16.3	0.7	74.28	222.36
40–75	581.7	185.4	82.8	7.7	0.6	13.6	7.6	15.7	6.5	0.6	86.12	98.70
75–120	610.7	179.4	70.0	6.8	0.8	14.3	5.0	24.8	4.1	0.4	84.15	73.53
135	660.0	161.3	58.5	5.2	0.7	13.8	12.2	22.1	16.5	0.5	76.06	234.61
215	621.0	169.4	76.6	7.3	1.3	20.7	12.5	30.2	16.7	0.7	74.04	171.23

[a] CIA (chemical index of alteration) = (100) $[Al_2O_3/(Al_2O_3 + CaO + Na_2O + K_2O)]$.
[b] CTR (calcium/titanium ratio) = (100) CaO/TiO_2.

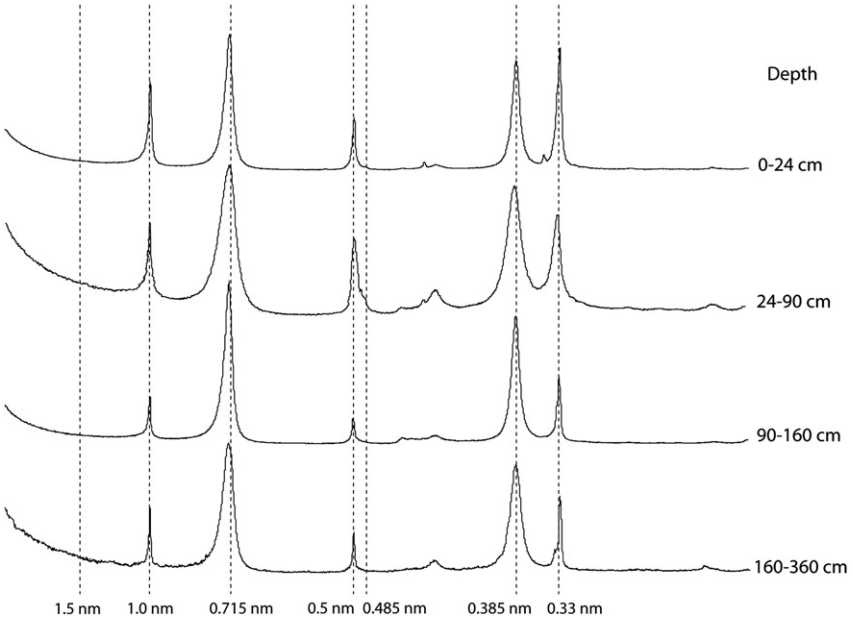

Fig. 5. XRD patterns (air-dried, oriented glass slides) of the <2 μm fraction of the soil and upper saprolite horizons of profile LS1.

plagioclases and biotites) incorporated into a secondary plasma rich in Fe-oxides (mainly released from the oxidation of structural iron in biotite) (Fig. 4d). Quartz and muscovite are unaltered; lithorelicts of K-feldspar are frequent throughout the plasmogenic matrix.

Micromorphological observations in upper Bt (argic) horizons (not illustrated) reveal the same characteristics as in the fine saprolite, but lithorelicts of K-feldspar and biotites are less common. The abundance of clay coatings, adjacent to the lithorelicts or incorporated into the secondary plasma, shows that illuviation is a significant pedogenic process in this interval.

4.2.3. Geochemical characteristics and weathering intensity

CIA values from profile PA1 (Table 2) indicate medium to high weathering intensity, from 81 in the top soil to 92 in the fine saprolite. The lower CIA values in the upper soil horizons are mainly ascribable to: (i) lower Al_2O_3 content, which itself is a consequence of clay migration or "lessivage" process occurring in the soil profile; (ii) higher K_2O content, which is probably the consequence of the biological cycling of K through litter fall decomposition of semi-deciduous forest vegetation. CTR values are >0 in all horizons.

The results of selective dissolution procedures (Table 3) corroborate those of the total analysis: the content of extractable CBD Fe is medium to high, with Fe_d/Fe_T ratio >60%, but in lower proportion than in the weathering profiles of the humid massif. Conversely, the amount of poorly crystallized Fe oxides, as deduced from oxalate extractant, here corresponds to higher proportion of the "free iron", with Fe_o/Fe_d ratio increasing toward the soil surface.

4.2.4. Weathering product mineralogy

XRD patterns of the clay fraction in profile PA1 indicate homogenous weathering product mineralogy from fine saprolite to upper soil horizons (Fig. 6). Well-crystallized kaolinite (WCK) was recorded

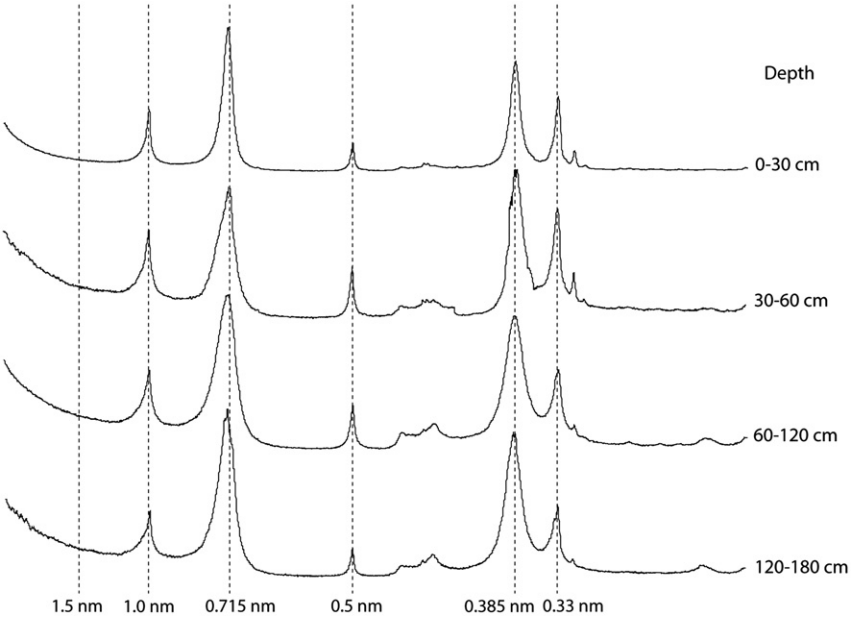

Fig. 6. XRD patterns (air-dried, oriented glass slides) of the <2 μm fraction of the soil and upper saprolite horizons of profile PA1.

as the dominant clay mineral, but high amounts of illite were also detected and consist of two populations: (i) well crystallized illite (WCI) with peaks at 1.00 and 0.50 nm, and (ii) poorly crystallized illite (PCI), indicated by the low-angle shoulder of the illite peak at 1.05 nm after decomposition of the XRD spectra.

According to Meunier and Velde (2004), the WCI would correspond to a detrital, mica-precursor primary phase which has been poorly altered (here: muscovite). PCI would represent the "illitic" secondary phase derived from the weathering of the primary rock-forming minerals – namely, biotites and feldspars – by transformation and/or neoformation processes.

4.3. Soil and subsurface weathering facies of the semiarid piedmont ($0<WBI<50\ mm\cdot y^{-1}$)

4.3.1. Profile morphology and chemistry

The CA1 soil profile is located in a small quarry near Canindé, in the western part of the semi-arid erosional piedmont (S 4°22.301′, W 39°18.271′). Situated at the top of a flat interfluve at 200 m a.s.l., it comprises an organic horizon A1, a stone line, an argic horizon (Bt), and finally a transitional horizon (BC) with the gneissic grus (C) in which the dry consistence increases with depth (Fig. 4e)

H_2O pH values range from 6.2 to 7.1, with an increasing gradient with depth where soil pH is close to neutrality (Table 1). The moderate to high exchange capacity in all soil horizons (>24 cmol (+) kg^{-1} of clay) indicates a predominance of high-activity clays. Soil profile CA1 classifies as a Haplic Luvisol (chromic) (IUSS Working Group WRB, 2006).

4.3.2. Micromorphological characterization of weathering

Micromorphological analyses from profile CA1 show that the grus preserves the rock structure despite the fact that biotite and plagioclase are partly weathered and filled with a primary plasma corresponding to their own alteration products (Fig. 4f). When present, K-feldspars and antiperthite patches are mostly unaltered. By contrast, plagioclase crystals exhibit numerous dissolution cavities partly filled with neoformed illite (Fig. 6d; verified by SEM-EDS analysis and X-ray element mapping: see Bétard et al., 2009 for more details).

Weathering of plagioclase and biotite gradually increases from the weathered gneiss to the soil surface. In BC and Bt horizons, K-feldspar and anthiperthite are intensely weathered and incorporated into the plasmogenic matrix. Amorphous plasma is absent in the grus material (C horizon).

4.3.3. Geochemical characteristics and weathering intensity

CIA values calculated from total element analysis in profile CA1 (Table 2) indicate low to medium weathering intensity, ranging between 74 and 76 at 135 and 215 cm depths, respectively. Such values are also in agreement with typical CIA values recorded in grus-type weathering mantles (Migoń and Thomas, 2002). CTR values are highly positive in all horizons, with a slight decrease in Bt and BC horizons.

The lower weathering intensity is confirmed by selective dissolution data, which reveal much lower concentrations of free iron (Fe_d/Fe_T ratio ≤20%) in the grus material (Table 3). Unlike the fine saprolites of the humid and subhumid zones, structural Fe of the primary rock-forming (e.g., biotite, garnet) and secondary clay minerals (iron-rich clays) is the dominant form of Fe in the grus weathering mantles covering the semiarid piedmont. The proportion of "free iron" increases in subsurface samples, with a maximum of 50.36% in Bt horizon.

4.3.4. Weathering product mineralogy

XRD patterns from profile CA1 (Fig. 7) show that 2:1 minerals (smectite and illite) are the major components of the soil clay-mineral assemblage. However, diffraction patterns reveal that 1:1 minerals are also present and appear to be more prevalent toward the surface. In detail, the <2 μm fraction of soil and grus samples exhibits a paragenesis of clay minerals comprising: (i) smectite, with AD peaks at 1.50 and 0.70 nm that shift in EG state to 1.70 and 0.85 nm, respectively; (ii) WCI, with peaks at 1.00 and 0.50 nm; (iii) PCI, shown by a shoulder in the illite peak at 1.05 nm; (iv) well crystallized kaolinite (WCK), with peaks at 0.715 and 0.385 nm; and (v) poorly crystallized kaolinite (PCK), as shown by the low-angle shoulder of the kaolinite peak at 0.725 nm. A formamide test (Churchman et al., 1984) performed on these samples did not reveal any presence of halloysite.

The same paragenesis of clay minerals was found in profile RE1 (not illustrated), but mixed-layer illite–smectite (IS) was detected here in higher amounts. Vermiculite was also identified, with an AD peak at 1.4 nm that did not shift in EG state. It was formed in association with the dominant smectite-type clay minerals which predominantly result from the weathering of biotite.

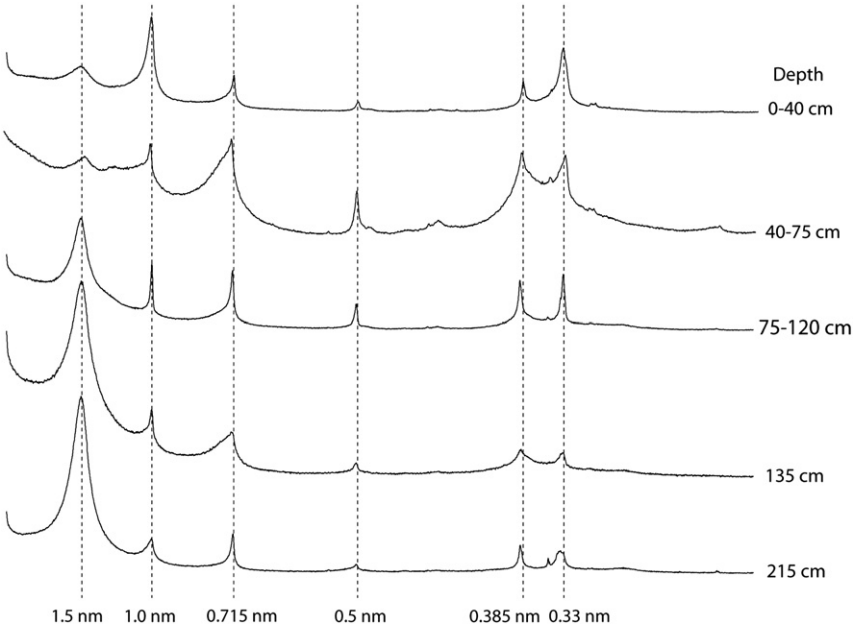

Fig. 7. XRD patterns (air-dried, oriented glass slides) of the <2 μm fraction of the soil and upper grus horizons of profile CA1.

5. Discussion

5.1. Soil-weathering system response to present-day water balance variations

With the combined help of field observations and laboratory results, a synthetic map showing the different types of soil weathering was drawn up for the Baturité massif and its piedmont (Fig. 8). The main WBI curves were traced on the same map to highlight the possible relationships between soil weathering processes and present-day water balance variations. The results clearly show a high spatial correlation between the distribution of hydrolytic weathering and the current pedoclimatic conditions: (i) in the humid massif ($WBI > 500\ mm \cdot y^{-1}$), monosiallitization is exclusive and leads to the neoformation of 1:1 clay minerals (kaolinite) with minor amounts of gibbsite; (ii) in the subhumid peripheral area of the massif ($50 < WBI < 500\ mm \cdot y^{-1}$), monosiallitization coexists with bisiallitization, producing a mixture of 1:1 (kaolinite) and 2:1 (illite) clay minerals; (iii) in the semiarid piedmont ($0 < WBI < 50\ mm \cdot y^{-1}$), bisiallitization becomes the dominant weathering pathway, with the most vulnerable primary minerals weathered into high-charge, 2:1 secondary clays (smectite and illite). This correlation between weathering types and water-balance variations is very similar to that observed in the gneissic uplands of Karnataka in peninsular India, between the kaolinite-dominated and smectite-dominated core areas of a well-characterized climosequence (Gunnell, 2000; Gunnell and Bourgeon, 1997).

In fact, it is mainly through the quantity of water which percolates into the weathering system ("climatic drainage") that the climatic control exercises its influence on weathering processes in tropical regions (Bourgeon and Pédro, 1992; Pédro, 1968). When hydrolysis is the prominent way of weathering as is the case in the study area, the development of a particular process (mono- or bi-siallitization) depends on the rate of removal of silica and basic cations, which itself is influenced by the amount of water flowing into the weathering system. This explains the good spatial correlation between weathering types and WBI envelopes (Fig. 8). Indeed, the WBI curve of 500 mm corresponds exactly to the domain of exclusive monosiallitization, with high values of deep drainage leading to fine saprolite formation and total dealkalination in the soil profiles. Below 50 mm of mean annual deep percolation, partial hydrolysis leads to bisiallitization and correlative grus formation conditioned by low, but irregular, deep drainage along with incomplete dealkalination. Above the grus weathering mantle, the red Luvisols covering the interfluves of the semi-arid piedmont are typical of a fersiallitic pedogenesis, which involves high contents of "free iron" (≥50% in Bt horizon) and the prevalence of 2:1 clays in the soil mineral assemblage (Duchaufour, 1982). Finally, between 50 and 500 mm of deep drainage, the areas of mono- and bi-siallitization overlap, that can be explained by intermediate conditions of weathering intensities. Such a progressive increase of weathering intensity from semiarid to humid conditions is also illustrated by the linear correlation between CIA values and the relative quantity of iron released during weathering (Fig. 9).

5.2. Soil-weathering system response to Quaternary paleoclimatic changes

Clearly, the formation of soils and weathering mantles is not an instantaneous phenomenon and requires long time periods to develop. According to Lageat and Gunnell (2001), tropical soils and weathering mantles may be considered as palimpsests reflecting "average" bioclimatic conditions that prevail at timescales of 1 to 10 Myr. Thus the duration of the Quaternary period appears to be an order of magnitude likely to control soil and saprolite development, given the propagation rates of weathering fronts estimated for tropical regions (1 to $10\ m \cdot Ma^{-1}$: Boeglin and Probst, 1998; Braun et al., 2005; Théveniaut and Freyssinet, 1999; Thomas, 1994).

Based on existing palaeoclimatic studies in northeastern Brazil, it seems that, here as in other areas of the tropics, several dry and wet phases have occurred since the Late Tertiary, although it is not currently possible to establish a precise chronology for the last ten million years. But three trends in the paleoclimate record have affected the northeast of Brazil during the Quaternary: (i) the existence of wet periods occurring on brief intervals over the past 200 kyr at least (Wang et al., 2004); (ii) the intervention of more arid phases during the Pleistocene, as evidenced by the widespread deposition of aeolian sand covers on the piedmont zones (Barreto et al., 2004; Bétard, 2007) (iii) the prevalence of climatic conditions similar to those of today throughout the Quaternary (Behling et al., 2000) and, more broadly, over the last 13 Myr (Harris and Mix, 2002).

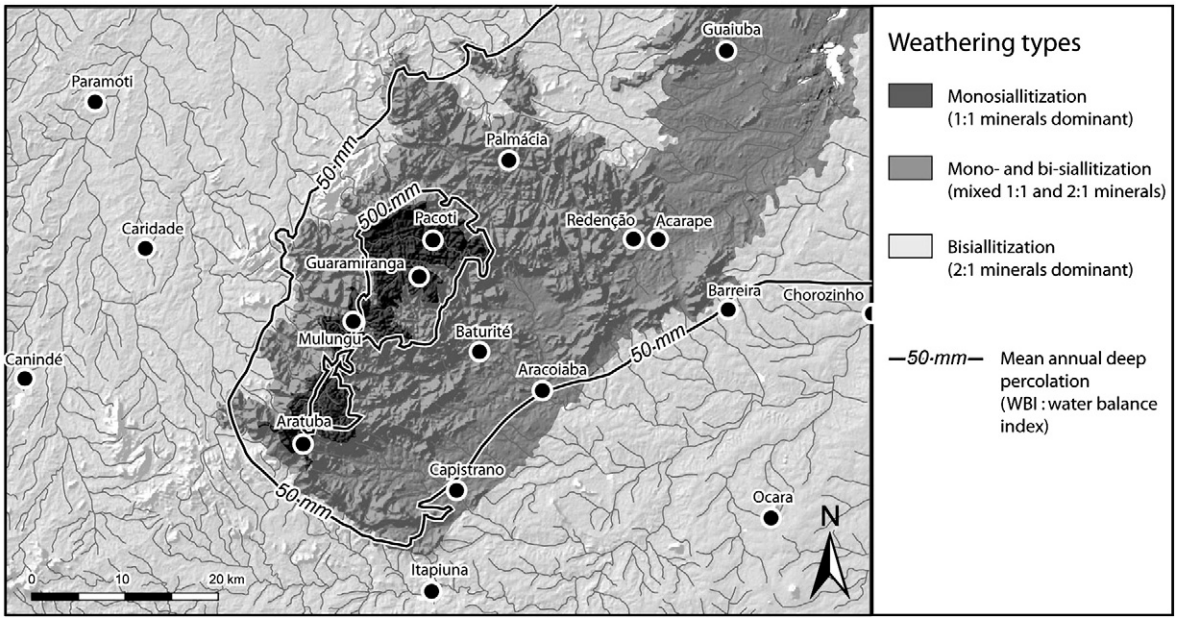

Fig. 8. Distribution of soil weathering processes in the study area.

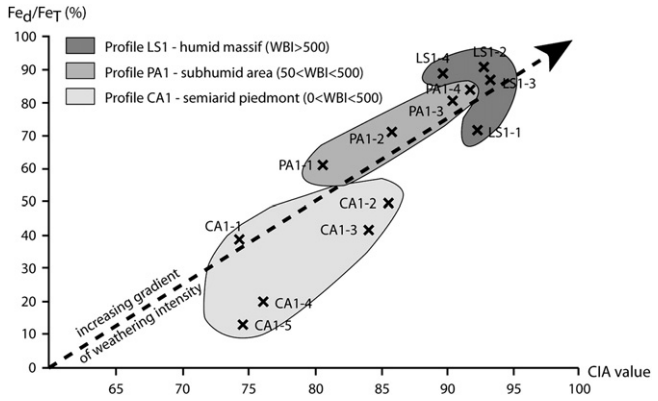

Fig. 9. Weathering intensity in the study area: highlight of correlation between CIA (Chemical Alteration Index) values and the Fe_d/Fe_T ratio, for the three selected profiles.

These considerations lead to the assumption that the geochemical pathways of soil weathering and their distribution in the study area are reflective of inevitable, long-term (Quaternary to Neogene) climatic fluctuations around statistical median values close to the present ones. Modelling the effects of such changes on the soil-weathering system is much more difficult, even if some features identified in the field may be a function of drier or wetter palaeoclimates. For example, the mid-slope plinthite identified in several soil profiles of the humid massif, as well as some terrace deposits rich in rounded quartz pebbles found 10–15 m m above the present-day valley floor, are probably indicative of drier or more contrasted climates with distinct wet and dry seasons. Paleoclimatic legacies of the Palaeogene lateritization event (Tardy and Roquin, 1998) are rare, but the archives of such a palaeoweathering stage seem mainly contained in the Neogene clastic sediments of the Barreiras Formation that underline the pre-littoral tablelands (Bétard, 2007; see below).

5.3. Soil-weathering system response to long-term denudation

In situ soil profile thickness and evolution depend on the balance between water–rock interaction processes at the weathering front and soil stripping processes at the surface by mechanical erosion, which itself is conditioned by tectonic activity and related denudation rates (Bourgeon and Gunnell, 1998). In the northern Brazilian "Nordeste", tectonic regime is dominated since the Late Cretaceous by a large-scale flexural uplift with its crest situated at ~300 km from the coastline (Peulvast et al., 2008). Denudational response to post-rift crustal uplift corresponded to the progressive exhumation of a wide, shallow embayment on the northern flank of the flexure (the "sertaneja" depression), with mean erosion rates of 7 to 10 $m \cdot Ma^{-1}$ over post-Cenomanien times. Similar erosion rates were deduced for the Late Cenozoic from the measured thickness of the Neogene clastic sediments (onshore Barreiras and offshore Tibau formations) extending over the continental margin of Ceará (Peulvast et al., 2008).

The geomorphic consequence of that long-term uplift trend was to rejuvenate continuously the landsurface through climatically-controlled cycles of etching and stripping (Thomas, 1989). After a humid phase a chemical denudation leading to laterite formation in Early Tertiary times (Tardy and Roquin, 1998), a marked shift towards aridity began at ~13 Myr (Harris and Mix, 2002), favoring soil stripping and the development of a refreshed landsurface (Gunnell, 1998). Indeed, this period of increased aridity regionally coincides with the deposition of the Barreiras sediments, a detrital formation locally rich in quartz pebbles, inherited kaolinite and ferruginous gravels (Bétard, 2007). Combined with the presence of truncated weathering profiles and bare rock surfaces below the unconformable Barreiras sediments, there is strong sedimentological evidence in the study area that the pre-Neogene paleoweathering profiles were severely scoured to the lowermost regolith horizons in the erosional piedmont. Vestiges of Paleogene laterites have been observed at higher elevations in the landscape, mainly outside of the limits of the study area (Pereiro massif, Araripe-Campos Sales area: Bétard et al., 2005). They remain currently scarce in the geomorphic environment of the Baturité massif because persistent epirogenic uplift and proximity to the base level have promoted the rapid mechanical erosion of most of the inherited kaolinite mantle and upper lateritic landforms. Stripping of the paleoweathering mantle finally steered the landscape towards new forms of weathering and pedogenesis in the piedmont zone, with the newly established semi-arid conditions favouring grus formation and fersiallitic pedogenesis.

6. Conclusion

In the northern Brazilian "Nordeste", the Baturité massif serves as a natural laboratory for analysing the morphological, geochemical and mineralogical variations experienced by soil and subsurface weathered materials in a tropical mountain characterized by a steep environmental gradient. By using different scales of observation, from field scale to micromorphology, this study gives some contributions to the understanding of spatial variations and co-evolutions of soil and subsurface weathering properties. Of particular relevance to the aim of this study, the results reveal a close spatial correlation between the distribution of soil weathering processes and present-day water balance (or pedoclimatic) variations, from monosiallitic weathering in the humid summit zone ($WBI > 500\ mm \cdot y^{-1}$) to bisiallitic weathering in the semi-arid piedmont ($WBI < 50\ mm \cdot y^{-1}$).

Beyond the question of spatial variability addressed in this paper, temporal variability of soil and weathering mantle formation is still poorly characterized, e.g. in obtaining constraints on the exact timing of weathering process and the propagation rate of weathering fronts. Further works in the study area will be dedicated to a better characterization of weathering-mantle-stratigraphy coupled with relative or absolute dating techniques, such as palaeomagnetism on hematite (Théveniaut and Freyssinet, 1999) and/or (U-Th)/He analysis of goethite (Shuster et al., 2005).

Acknowledgements

This study would not have been possible without the funding and material assistance by the LGP (Laboratoire de Géographie Physique, UMR CNRS 8591), the HydrASA laboratory (Hydrogéologie, Argiles, Sols et Alterations, UMR CNRS 6269) and the UFC (Universidade Federal do Ceará, Fortaleza). It has benefited from previous helpful discussions with Jean-Pierre Peulvast (Paris-Sorbonne University) and Yanni Gunnell (Paris-Diderot University). Help in the field work by Gérard Bourgeon (CIRAD) and in the laboratory by Laurent Caner (HydrASA) was also gratefully appreciated. We finally thank the two anonymous referees for their constructive comments on the submitted manuscript.

References

Barreto, A.M.F., Suguio, K., Bezerra, F.H.R., Tatumi, S.H., Yee, M., Giannini, P.C.F., 2004. Geologia e geomorfologia do Quaternário Costeiro do Estado do Rio Grande do Norte. Geologia USP Série Científica, São Paulo 4 (2), 1–12.

Behling, H., Arz, H.W., Pätzold, J., Wefer, G., 2000. Late Quaternary vegetational and climate dynamics in northeastern Brazil, inferences from marine core GeoB 3104–1. Quaternary Science Reviews 19, 981–994.

Bétard, F., 2007. Montagnes humides au cœur du Nordeste brésilien semi-aride: le cas du massif de Baturité (Ceará). Apports d'une approche morphopédologique pour la connaissance et la gestion des milieux. Ph.D. thesis (unpublished), Paris-Sorbonne University, France.

Bétard, F., Peulvast, J.P., Claudino Sales, V., 2005. Laterite preservation and soil distribution in the Araripe-Campos Sales area: consequences of uplift, erosion and climatic change. 6th International Conference on Geomorphology, Zaragoza, p. 69 (Abstracts Volume).

Bétard, F., Caner, L., Gunnell, Y., Bourgeon, G., 2009. Illite neoformation in plagioclase during weathering: evidence from semi-arid Northeast Brazil. Geoderma 152, 53–62.
Blakemore, L.C., Searle, P.L., Daly, B.K., 1987. Methods for Chemical Analysis of Soils. New Zealand Soil Bureau Scientific Report 80, Lower Hutt.
Boeglin, J.L., Probst, J.L., 1998. Physical and chemical weathering rates and CO_2 consumption in a tropical lateritic environment: the upper Niger basin. Chemical Geology 148, 137–156.
Bourgeon, G., 2001. A survey of soil and weathering patterns through land system mapping in the Western Ghats region. In: Gunnell, Y., Radhakrishna, B.P. (Eds.), Sahyadri, the great escarpment of the Indian subcontinent. Patterns of landscape development in the Western Ghats. Geological Society of India, Gavipuram, pp. 855–904.
Bourgeon, G., Gunnell, Y., 1998. Rôle du régime tectonique et du taux de dénudation sur la répartition géographique et les propriétés des sols tropicaux. Comptes-rendus de l'Académie des Sciences de Paris 326, 167–172.
Bourgeon, G., Pédro, G., 1992. Rôle majeur du drainage climatique dans la différenciation altéritique et pédologique des sols des régions chaudes. Comptes-rendus de l'Académie des Sciences de Paris 314, 717–725.
Braun, J.J., Ngeoupayou, J.R.N., Viers, J., Dupré, B., Bedimo, J.P., Boeglin, J.L., Robain, H., Nyeck, B., Freydier, R., Nkamdjou, L.S., Rouiller, J., Muller, J.P., 2005. Present weathering rates in a humid tropical watershed: Nsimi, South Cameroon. Geochimica et Cosmochimica Acta 69, 357–387.
Churchman, G.J., Whitton, J.S., Claridge, G.G.C., Theng, B.K.G., 1984. Intercalation method using formamide for differentiating halloysite from kaolinite. Clays and Clay Minerals 32, 241–248.
CPRM, 2003. Atlas digital de geologia e recursos minerais do Ceará. Mapas na escala 1:500,000. Serviço Geológico do Brasil (CD-Rom).
Duchaufour, Ph., 1982. Pedology: pedogenesis and classification. Allen & Unwin, London, Boston.
Ehlen, J., 2005. Above the weathering front: contrasting approaches to the study and classification of weathering mantle. Geomorphology 67, 7–21.
Gunnell, Y., 1998. Passive margin uplifts and their influence on climatic change and weathering patterns of tropical shield regions. Global and Planetary Change 18, 47–57.
Gunnell, Y., 2000. The characterization of steady state in Earth surface systems: findings from the gradient modelling of an Indian climosequence. Geomorphology 35, 11–20.
Gunnell, Y., Bourgeon, G., 1997. Soils and climatic geomorphology on the Karnataka Plateau, peninsular India. Catena 29, 239–262.
Harris, S.E., Mix, A.C., 2002. Climate and tectonic influences on continental erosion of tropical South America, 0–13 Ma. Geology 30, 447–450.
IUSS Working Group WRB, 2006. World Reference Base for Soil Resources 2006, World Soil Resources Report No. 103, 2nd edition. FAO, Rome.
Lageat, Y., Gunnell, Y., 2001. Landscape development in tropical shield environments. In: Godard, A., Lagasquie, J.J., Lageat, Y. (Eds.), Basement regions. Springer, Berlin, pp. 173–197.
Mehra, O.P., Jackson, M.L., 1960. Iron oxide removal from soils and clays by a dithionite-citrate buffered with sodium carbonate. Clays and Clay Minerals 7, 317–327.
Meunier, A., Velde, B., 2004. Illite: Origin, Evolution and Metamorphism. Springer, New York.
Migoń, P., Thomas, M.F., 2002. Grus weathering mantles – problems of interpretation. Catena 49, 5–24.
Monié, P., Caby, R., Arthaud, M.H., 1997. The Neoproterozoic Brasiliano orogeny in Northeast Brazil: $^{40}Ar/^{39}Ar$ and petrostructural data from Ceará. Precambrian Research 81, 241–246.
Nesbitt, H.W., Young, G.M., 1989. Formation and diagenesis of weathering profiles. Journal of Geology 97, 129–147.
Pédro, G., 1968. Distribution des principaux types d'altération chimique à la surface du globe. Revue de Géographie Physique et de Géologie Dynamique 10, 457–470.
Peulvast, J.P., Claudino Sales, V., 2004. Stepped surfaces and palaeolandforms in the northern Brazilian "nordeste": constraints on models of morphotectonic evolution. Geomorphology 62, 89–122.
Peulvast, J.P., Claudino Sales, V., Bétard, F., Gunnell, Y., 2008. Low post-Cenomanian denudation depths in the Brazilian Northeast: implications for long-term landscape evolution at a transform continental margin. Global and Planetary Change 62, 39–60.
Price, J.R., Velbel, M.A., 2003. Chemical weathering indices applied to weathering profiles developed on heterogeneous felsic metamorphic parent rocks. Chemical Geology 202, 397–416.
Projeto Radambrasil, 1981. Levantamento integrado dos recursos naturais do Brasil. Folha Jaguaribe-Natal. Ministério das Minas e Energia-MME, Rio de Janeiro.
Scarciglia, F., Le Pera, E., Critelli, S., 2005. Weathering and pedogenesis in the Sila Grande Massif (Calabria, South Italy): from field scale to micromorphology. Catena 61, 1–29.
Shaw, R., 1997. Variations in sub-tropical deep weathering profiles over the Kowloon granite, Hong Kong. Journal of the Geological Society 154, 1077–1085.
Shuster, D.L., Vasconcelos, P.M., Heim, J.A., Farley, K.A., 2005. Weathering geochronology by (U-Th)/He dating of goethite. Geochimica et Cosmochimica Acta 69, 659–673.
Tardy, Y., Roquin, C., 1998. Dérive des continents. Paléoclimats et altérations tropicales. Éditions du BRGM, Orléans.
Théveniaut, H., Freyssinet, Ph., 1999. Paleomagnetism applied to lateritic profiles to assess saprolite and duricrust formation processes: the example of Mont Baduel profile (French Guiana). Palaeogeography, Palaeoclimatology, Palaeoecology 148, 209–231.
Thomas, M.F., 1989. The role of etch processes in landform development: II. Etching and the formation of relief. Zeitschrift für Geomorphologie 33, 257–274.
Thomas, M.F., 1994. Geomorphology in the tropics. A study of weathering and denudation in low latitudes. J. Wiley & Sons, Chichester.
Wang, X.F., Auler, A.S., Edwards, R.L., Cheng, H., Cristalli, P.S., Smart, P.L., Richards, D.A., Shen, C.C., 2004. Wet periods in northeastern Brazil over the past 210 kyr linked to distant climate anomalies. Nature 432, 40–43.